J Vis (2020) 23:395–408
https://doi.org/10.1007/s12650-020-00640-3

REGULAR PAPER

A. Matthujak · C. Kasamnimitporn · T. Sriveerakul

Comparative visualized investigation of impact-driven high-speed liquid jets injected in submerged water and in ambient air

Received: 23 July 2019 / Revised: 27 January 2020 / Accepted: 3 March 2020 / Published online: 19 March 2020
© The Visualization Society of Japan 2020

Abstract This paper is a comparative study on the characteristics of high-speed liquid jets injected in surrounding water and air using shadowgraph technique. One of the main objectives is to investigate the effects of liquid's physical properties, used to generate the high-speed liquid jets, on jet generation's characteristics. Moreover, comparative investigations on effects of those liquid jets after injected in water and air are reported. The high-speed liquid jets were generated by the impact of a projectile launched by a horizontal single-stage power gun. The impact-driven high-speed liquid jets were visualized by shadowgraph technique and images were recorded by a high-speed digital video camera. The process of impact-driven high-speed liquid jet injection in air and water, oblique shock waves, jet-induced shock waves, shock waves propagation, the bubble behavior, bubble collapse-induced rebound shock waves and bubble cloud regeneration were clearly observed. It was found that different properties of liquid (surface tension and kinematic viscosity) affect the jet maximum velocity and shape of the jet. Bubble behaviors were only found for the jet injected in water. From the shadowgraph images, it is found that the maximum average jet velocity, expansion and contraction velocities of bubble in axial direction increase when the value of the multiplied result of surface tension by kinematic viscosity increases. Therefore, surface tension and kinematic viscosity are the significant physical properties that affect characteristics of high-speed liquid jets.

Keywords High-speed liquid jets · Impact-driven method · Physical properties of liquid · Shadowgraph · Shock wave · Bubble

1 Introduction

The study of high-speed liquid jets was initiated regarding the impact of rain droplets on high-speed vehicles (Methven and Fairhead 1959; Westmark and Lawless 1995; Kennedy and Field 2000; Deom et al. 2005). This topic was subsequently extended to a wide range of engineering applications including cavitation research (Lesser and Field 1991; Bourne and Field 1995), jet cutting and jet cleaning technology, mining and tunneling by means of high-speed jet impingements (Bowden and Field 1964; Kobayashi et al. 1988; Shi et al. 1994a; Obara et al. 1995a; Crafton et al. 2006), fire extinguishers, diesel fuel injection (Shi et al. 1994b; Lee and Park 2002; Milton and Pianthong 2005a), gasoline fuel injection (Shimotani et al. 1996; Wang et al. 2006) and supersonic combustion ram jet engines (Ferri 1964; Terao et al. 2002).

However, the liquid jets that were produced traditionally by discharging liquid through a nozzle or an orifice connected to pressurized liquid chambers at static pressures of sub-GPa had a technical limitation. To overcome such technical limitation, Bowden and Brunton (1958, 1961) generated extreme high-pressure

A. Matthujak (✉) · C. Kasamnimitporn · T. Sriveerakul
Combustion and Jet Application Research Laboratory, Department of Mechanical Engineering, Faculty of Engineering, Ubon Ratchathani University, Ubon Ratchathani 34190, Thailand
E-mail: Anirut.m@ubu.ac.th

water jet using the impact of high-speed projectiles against a liquid-filled container. A water jet of 1200 m/s was produced and recorded using a high-speed photography technique. The erosion of solid surfaces applied by the water jet impinge was the main focus of the study. Since then, extensive studies have been carried out by many researchers (Hawke 1989; Charters 1987; Grosch and Riegel 1993).

Following the work of Bowden and Brunton, O' Keefe et al. (1967) successfully applied explosive power to generate high-speed liquid jet based on the impact-driven method (IDM). A jet was set up and generated vertically by an explosive power. The jet's nozzle was made from steel which had 30° of core angle. When the projectile velocities of 0.714–1.90 km/s impacted the Laxan piston and water inside the tube, water was then driven into the nozzle. The flow behaviors of the generated hypersonic jet were observed such that the hypersonic water jet was generated at a maximum velocity of 4.58 km/s. Experimental visualization of the supersonic water jets was presented. Moreover, the motion of the water column in the converging tapered section was described by one-dimensional unsteady compressible flow equations. Ryhming (1973) presented an analysis study for the motion of a free fluid packet through a jet nozzle based on one-dimensional incompressible flow theory. The analysis study for the fluid motion when the fluid packet reaches the nozzle exit plane was also presented. However, both of the published papers (O'Keefe et al. 1967; Ryhming 1973) did not consider either shock wave or wave reflection within the nozzle.

Glenn (1975) numerically described the mechanics of the impulsive water cannon based on unsteady compressible fluid flow equations. Comparisons of the calculation results, both with Rhyming's study (Ryhming 1973) and with his own experimental results, were also displayed. However, in both Rhyming's and Glenn's study, the physical model and the experimental setups were slightly different from the Bowden and Brunton's method. This is because the water packet was initially accelerated by a piston in a constant cross-sectional tube before passing through the empty section of a converging nozzle. Similar to O'Keefe's study, either the shock wave or the wave reflection within the nozzle was not considered.

Field and Lesser (1977) investigated experimentally and analytically supersonic liquid jet flows and predicted self-combustion of oil jets at high supersonic jet speeds. In 1992, Shi et al. (1994a, b, 1996; Shi and Itoh 1998) visualized high-speed liquid jets at supersonic to hypersonic speeds using double exposure holographic interferometry and studied effects of liquid jet impact on liquid and solid surface (Shi et al. 1994a, 1999; Shi and Itoh 1998), shock waves generation over high-speed jets (Shi et al. 1993; Shi and Takayama 1995) and auto-ignition feasibility of supersonic diesel fuel jet (Shi and Takayama 1999). The characteristics of jet velocity of up to 3 km/s were described, and it was claimed that the sign of auto-ignition was at 2 km/s diesel jet in atmospheric air. It was concluded that the temperature behind the shock wave at stagnation regions of a diesel fuel jet is high enough to induce the auto-ignition.

Subsequently, Pianthong (2002; Milton and Pianthong 2005b) studied the generation of supersonic liquid jets and jet-induced shock waves by using the shadowgraph method. This clarified the effect of nozzle geometries on jet speeds, jet shapes and shock wave angles (Pianthong et al. 2002). Particularly, the analysis of multiple-pulsed supersonic diesel jet formation (Pianthong et al. 2003a, 2005) based on a simple one-dimensional model (Pianthong et al. 2003b) was first performed. A negative result regarding the induction of auto-ignition over a 2 km/s diesel fuel jet in atmospheric air was obtained in this study.

Milton et al. (2005) presented the simulation of supersonic liquid jets by using a 2D Autodyne code. The mechanism of shock waves and shock wave reflection occurring inside a nozzle after projectile impact and the pulsing of a supersonic jet were shown. However, the phenomena occurring in the nozzle cavity, which were related to jet characteristics, has never been clarified. Although there have been some analytical and numerical descriptions attempted to clarify such phenomena, the experimental results are still needed for verification.

Most of the studies of high-speed liquid jets have handled only water and diesel. In 2007, therefore, Matthujak et al. (2007) experimentally studied the effect of different liquid jets on jet characteristics using high-speed video recordings of shadowgraph images. Impulsive water, diesel, bio-diesel, kerosene and gasoline jets at jet speeds ranging from 1.3 to 2.3 km/s were generated by the impact-driven method. It was found that the physical properties of each liquid jet were significant factors in the differences of jet formation, jet speed and jet penetration distance. Moreover, to verify the contribution of shock waves with jet formation, pressure measurement, double exposure holographic interferometric visualization and high-speed video recordings of shadowgraph images of waves propagating were included. It was found that (1) before the nozzle flow started, longitudinal and transversal waves and their reflected waves coalesced with a main impact generated shock wave; (2) the primary jet was driven by pressures caused by a projectile impingement; (3) successive shock reflections inside the container of liquid drove intermittent multiple liquid jets; and (4) the contribution of released longitudinal and transversal waves to multiple jet formation was marginal.

Recently, the attention of using high-speed liquid jets has begun to be focused not only for medical applications (drug injection, tissue cutting and removal of a cerebral thrombus) (Nakagawa et al. 2002; Hirono et al. 2003; Ohki et al. 2004), but also for industrial applications of jet to underwater work. Obara et al. (1995b) investigated the mechanisms of the liquid jet impact on liquid. A water jet with a diameter of 3 mm was generated using a single-impact jet apparatus. The water jet with impact speed at 600 m/s was applied on the surface of water. In the impact upon a water surface, a cavitation bubble cloud generated at the central axis of the liquid jet and the release wave produced by the reflection of the shock wave at the interface were visualized using the shadowgraph technique. Moreover, it was observed that the generation of the cavitation bubble and its rapid collapse might contribute to damage of the impacted surface. That was because the bubble collapse might produce localized pressure concentrations on a material surface due to micro-jet impact. However, the behaviors of a jet-generated bubble and its collapse were not clearly described in the study.

Soyama et al. (1996) described the phenomena occurring around ultrahigh-speed submerged water jet. Continuous water jets with maximum injection pressure of 70 MPa and flow rate of 22 l/min were generated by a plunger pump. The water jet accompanied by very severe cavitation was visualized using shadowgraph technique, and impulsive pressures around the jets were measured by means of a pressure-sensitive film. The effects of the injection pressure and the nozzle configuration on the impulsive pressure of the jet were also clarified.

Ohtani et al. (2009) reported the result of preliminary experiments of pulsed Ho:YAG laser-induced jets applied to drill a submerged rock specimen. The laser-induced water jets were visualized by a high-speed digital video camera using the shadowgraphs technique. The jet speed was estimated to be about 40 m/s from shadowgraph images. High stagnation pressures generated by jet impingements were also measured. It was found that simultaneously shock waves of about 22.7 MPa were generated at bubble collapse, which effectively cracked the surface of the rock specimens. Hence, it was concluded that repeated exposures of these laser-induced jets against submerged rock specimens have potential to practically bore holes on rock surfaces.

The previous studies of submerged jet speed was quite low due to the limitation of jet generation technique. Therefore, characteristics of high-speed jet submerged in water have not been clarified yet. Matthujak et al. (2013) described a preliminary investigation of the characteristics of high-speed water jets injected in water, being generated by the impact-driven method. The ensuing impact-driven high-speed water jets in the water were visualized by the shadowgraph technique, and the images were recorded by a high-speed digital video camera. The processes following such jet injection into water, the jet-induced shock waves, shock wave propagation, the bubble behavior, bubble collapse-induced rebound shock waves and bubble cloud regeneration were observed. Moreover, the impact pressure of high-speed water jet in water was measured by a polyvinylidene difluoride (PVDF) piezoelectric film. Two peak overpressures caused by the impingement of water jet and bubble were clarified by the PVDF pressure sensor related to visualization. However, the generalizable results were not clarified yet.

From the literature studies, characteristics of liquid jets at supersonic up to hypersonic range injected in air were clearly clarified by both experimental and theoretical studies, while only a preliminary study of high-speed water jet in water (Matthujak et al. 2013) was performed. The objective of this present work is to clarify the comparative effects of different physical properties of liquid jets on jet characteristics injected in both air and water. Four liquid jets consisting of water, diesel, kerosene and gasoline jets were generated by the impact-driven method using the same projectile velocity. The images of jets were visualized by shadowgraph technique, and images were recorded by a high-speed digital video. Moreover, the differences of jet characteristics in air and water were concluded.

2 High-speed liquid jet generation

In this study, high-speed liquid jets were generated by the impact-driven method (Bowden and Brunton 1958, 1961). Using this technique, the liquid contained inside the nozzle cavity was impacted by a high-speed projectile. As shown in Fig. 1, the nozzle was directly connected to the exit of the pressure relief section. The liquid was constrained in the nozzle by the use of a plastic diaphragm seal at its top and bottom. This diaphragm was very thin and of low strength as compared to the impact momentum from the projectile. Therefore, the momentum loss of the projectile due to the strength of this plastic seal can be neglected. Pressure in a liquid-filled nozzle was enhanced by a momentum transfer being created with a sudden

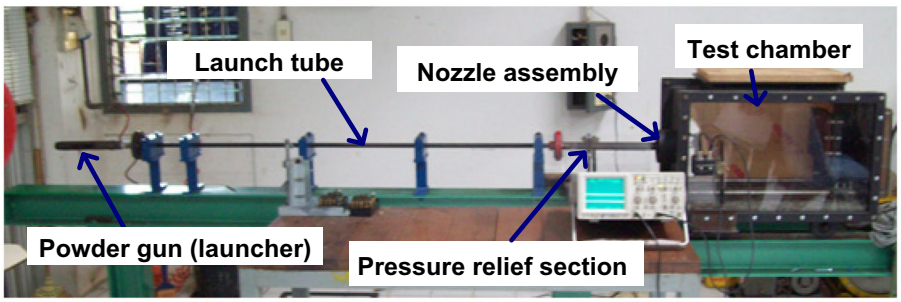

Fig. 1 Horizontal single-stage powder gun (HSSPG)

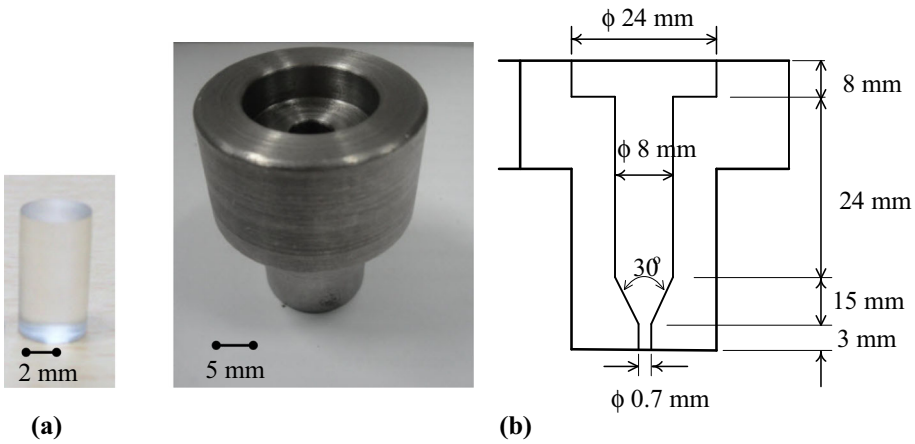

Fig. 2 **a** Projectile and **b** nozzle geometry

impingement of a high-speed projectile. The high-speed projectile needed in this technique was launched by the horizontal single-stage powder gun (HSSPG) as shown in Fig. 1. The HSSPG consisted of a launcher, launch tube, pressure relief section and test chamber. The launch tube had a diameter of 15 mm and a length of 1.5 m. The pressure relief section had a length of 38.5 cm, which was designed to diminish the blast wave in front of the projectile. The pressure relief section had four slots; each slot is 4 mm wide and 345 mm long. The test chamber was a square tank of 350 × 350 mm in width and 590 mm in length with two polymethyl methacrylate (PMMA) windows on two sides for visualization. The projectile was made of polymethyl methacrylate (PMMA) and is a cylindrical shape with a diameter of 15 mm, length of 8 mm and a weight of 0.92 g as shown in Fig. 2a. The HSSPG was employed to generate the high-speed liquid jet velocity of 550 to 2290 m/s in each gunpowder weights. The nozzle with exit diameter of 0.7 mm (Fig. 2b) that was connected to the pressure relief section was made of mid-steel. Gunpowder of 5 g was used in this study, which could launch the projectile to a speed of about 952 ± 4% m/s. Please note that at the smaller size of the nozzle, its friction loss could affect the jet formation or shock phenomena. However, this exit diameter of the nozzle is used with reference from past research (Pianthong 2002; Milton and Pianthong 2005b; Pianthong et al. 2002), where the maximum jet velocity can be reached.

3 Visualization method

A high-speed digital video camera and shadowgraph optical arrangement were used for visualization as shown in Fig. 3. The dynamic jet formations were quantitatively measured by sequential observations. A xenon lamp was used as a light source. The source light was collimated and passed through a concave lens and a circular slit. The laboratory space was limited, and therefore, the two plane mirrors of diameter 190 mm were combined. Two paraboloidal schlieren mirrors of diameter 300 mm were used for a collimating source light beam that passed the test section area. A Nikon 60-mm macro-lens was used to focus the

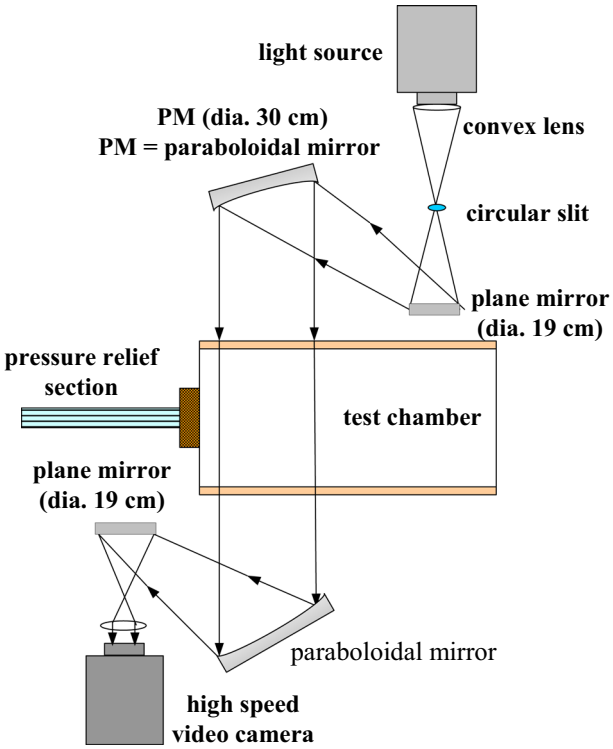

Fig. 3 Shadowgraph optical setup for high-speed digital video recording

object image on the high-speed digital video camera screen. The high-speed digital video camera was a Photron SA5 at a frame rate of up to 30,000 f/s, minimum shutter speed of up to 1 μs and 5.46 s record time at full resolution (640 × 376 pixels).

4 Results and discussions

4.1 Formation of liquid jets injected in air and water

Sequential shadowgraph images of water, diesel, kerosene and gasoline jets injected in air are shown in Fig. 4. Only 12 selected images of each jet at different time step are presented.

As in Fig. 4a1–d1 to a3–d3, the water jet had the slimmest width and more elongated than diesel, kerosene and gasoline jets, respectively. The diesel jet looked bulkier than other jets. The general trend of the kerosene jet formation was similar to the diesel jet formation while the gasoline jet generated with less penetration than other jets.

As observed in Fig. 4, the motions of all jets in air were supersonic so that oblique shock waves were created at the tips and also the jet's nodes. At the earlier stage, the inclination angle of the first oblique shock wave of water, diesel, kerosene and gasoline jets were about 15.5°, 17.5°, 20.0° and 24° which correspond theoretically to Mach number (M_s) of 3.74, 3.32, 2.92 and 2.46, respectively, whereas the observable jet speeds from high-speed images of those liquid jets were 1320.60 m/s (M_s = 3.88), 1161.44 m/s (M_s = 3.42), 1186.71 m/s (M_s = 3.48) and 1182.95 m/s (M_s = 3.48), respectively.

The jet speeds estimated from the shock inclination angle differed from those obtained from the video images. This was because the relationship between the oblique shock angle and a supersonic body is valid to a supersonic solid body. But in this case, the jet boundary consisted of distributed liquid droplets/air mixture and irregularly shaped liquid surface. Moreover, not only fragmentation from bulk liquid to droplets, but also atomization and vaporization on the liquid surface simultaneously took place. Therefore, the sound speed defined around such a jet boundary was no longer the same as that of air and slightly smaller than that in air as described in Matthujak's study (2007).

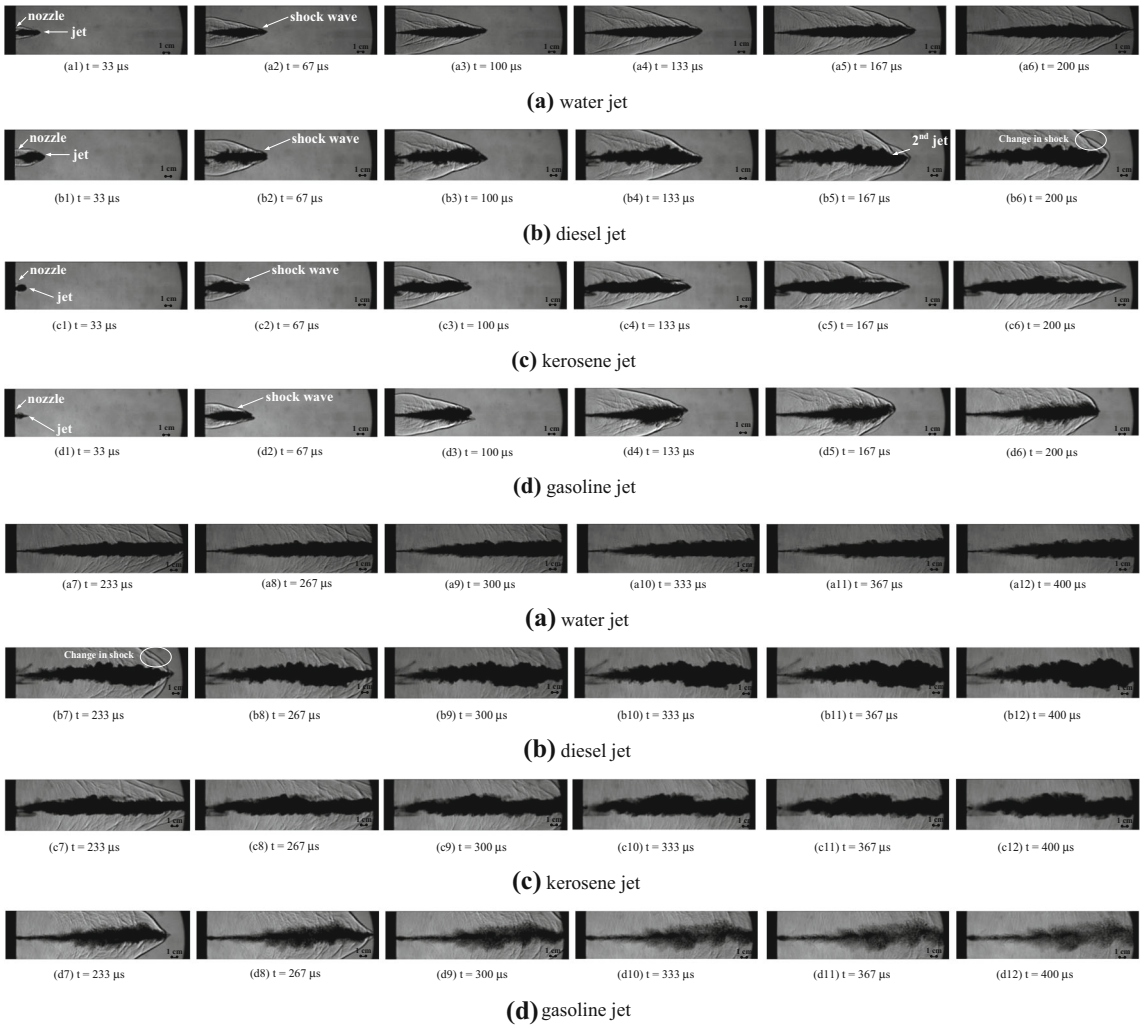

Fig. 4 Sequential shadowgraph images of jet formation injected in air

In Fig. 4a4–d4 to a6–d6, the water jet shape in air appears to be less disturbance than other jets. All jets were accelerated intermittently. The water jet speed was the fastest among other jets but its attenuation occurred very slightly with the elapse of time.

The diesel jet still looked bulkier than that of the water jet. This trend was commonly seen in kerosene and gasoline, which was attributable to smaller values of surface tension. In liquids having higher surface tension, the jet would not expand even at intermittent pressure loadings and the resulting sizes of nodes would be smaller. Moreover, two steps of impulsive jet as observed by the dramatic change in shock wave's angle were clearly observed in Fig. 4b5, b6. This might be due either to the accelerating and decelerating behavior during the jet flight or the higher velocity jet (the second pulsed jet) overtaking the first jet. This phenomena was previously explained by Matthujak et al. (2007) using experimental and analytical study. The results from the high-speed video visualization in this current study show good agreement with that explanation.

The kerosene jet formation was similar to the water jet formation with less atomization and longer penetration. A shear layer occurring around the gasoline jet was stronger than other jets. Not only the strong atomization and vaporization of gasoline jet, but also slow jet penetration was clearly observed. From estimation of all jet penetration distances at $t = 200$ µs in Fig. 4a6–d6, the average velocity of water jet was higher than that of kerosene, diesel and gasoline jets, respectively.

After 233 µs (Fig. 4a7–d7 to a12–d12), the water, diesel and kerosene jets were quite similar, being slim and has long penetration, even though the diesel jet was bulkier than water and kerosene jet. The change in

shock angle indicated that the two step impulsive jet was still observed in the diesel jet as shown in Fig. 4b7, b8. The strongest atomization, vaporization and the slowest penetration of the gasoline jet compared to other jets were observed.

Figure 5 shows sequential shadowgraph images of water, diesel, kerosene and gasoline jets injected in water. Only the selected 16 images are presented. In Fig. 5a1–d1 at 33 μs, after the projectile impacted the

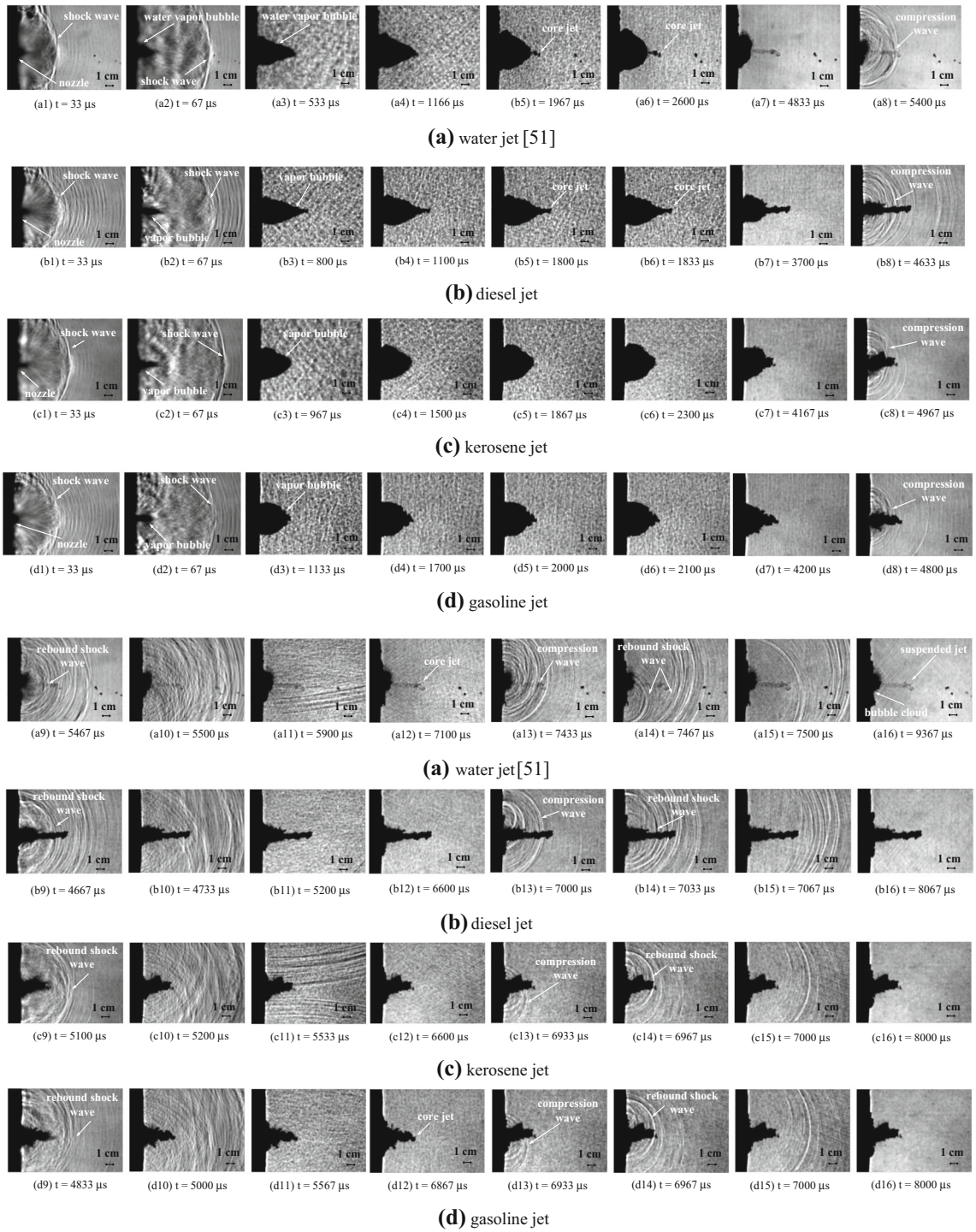

Fig. 5 Sequential shadowgraph images of jet formation injected in water

liquids contained inside a nozzle, the high-speed liquid jets contained vapor bubbles were discharged in quiescent water and the observable shock wave in water was generated and propagated along a test chamber.

Unlike the liquid jets injected in air, the vapor bubble generated by atomization and vaporization of the liquid jets expanded quickly as observed in a dark half ellipse shape (Fig. 5a2–d2 to a3–d3). They were created by the deflection of the collimated object beam through the bubble. Due to the localized steep density change at the vapor bubble, the collimated object beam was refracted at the bubble boundary so that the injected bubble has a dark shape. Although the increase in the bubble diameter was fast, it was slower than the increase in the bubble penetration distance in the jet axial. This implied that the jet penetration speed was faster than the expansion speed of the vapor bubble. The vapor bubbles were relatively thin at the beginning as shown in Fig. 5a2–d2, but it became thicker as the bubble diameter increased as shown in Fig. 5a3–d3. The vapor bubble of kerosene and gasoline jets was plumper than that of water and diesel jets. In Fig. 5a3–d3, the jet tips were attached with the bubble boundary in jet axial as the dark shape, so the maximum average velocity could be estimated by the elapsed time of the tip of a dark half ellipse shape. The maximum average velocity of the diesel jet was faster than that of water, kerosene and gasoline jets, respectively.

While the jets that contained the growing bubble penetrated to the maximum penetration distance as shown in Fig. 5a4–d4, the bubble diameter did not expand to the maximum diameter yet. It still kept continuously expanding around the jet. Considering the elapsed time in Fig. 5a4–d4, the growing bubble of the diesel jet penetrated to the maximum penetration distance before water, kerosene and gasoline jets, being 1100 μs, 1166 μs, 1500 μs and 1700 μs, respectively. It implied that the penetration velocity of diesel jet is faster than that of water, kerosene and gasoline, respectively. In Fig. 5a5–d5, after the bubbles penetrated to the maximum penetration distance, the bubble started to contract in the jet axial direction while the jets still penetrated forward and the bubble diameter also kept increasing. Thus, the bubbles were detached from the jet tips and they moved in opposite directions, which was clearly observed in water and diesel jets.

After expanding to the maximum bubble diameter as shown in Fig. 5a6–d6, the bubbles started to contract while the jets slowly penetrated forward and almost stopped penetration as observed in the core jet in Fig. 5a7–d7. The elapsed time of expanding to the maximum bubble diameter of diesel jet was less than that of kerosene, water and gasoline jets, being 1833 μs, 2300 μs, 2600 μs and 2600 μs, respectively. It implied that the expansion velocity of the diesel jet is fastest among other jets.

This contraction was driven because of the difference of the vapor pressure of the bubbles and the pressure of the surrounding water. In this stage, the bubble contracted in all directions. Before the bubble almost contracted to the minimum bubble volume, a compression wave was generated and propagated as shown in Fig. 5a8–d8.

The bubble of the diesel jet contracted to the minimum volume at 4467 μs, which was faster than kerosene, gasoline, kerosene and water jets, being 5067 μs, 5133 μs and 5467 μs, respectively, as shown in Fig. 5a9–d9. At the moment of minimum bubble volume, a rebound shock wave was generated due to bubble collapse, which the pressure built up inside the minimum bubble volume would become extremely high. The rebound shock wave propagated forward as shown in Fig. 5a9–d9 and Fig. 5a10–d10. This phenomenon can be described by cavitation mechanism.

Due to the extremely high pressure inside the bubble volume, not only the rebounded shock wave was generated, but also the bubble volume also increased as shown in Fig. 5a11–d11. In Fig. 5a11–d11 to a12–d12, the expansion and contraction mechanism of the bubble was indistinctly seen because the increase in the bubble volume was not obviously observed. However, such expansion and contraction mechanism were believed to occur due to the appearance of the compression wave, the rebounded shock wave and the shock wave propagation in Fig. 5a12–d12 to a13–d13, respectively. Such a mechanism could be similarly described as the previous mechanism in Fig. 5a1–d1 to a10–d10.

In Fig. 5a14–d14, there were other bubbles being separately generated. They expanded, contracted, collapsed and generated a rebound shock wave as well. Compared to the generation of the first and the second rebounded shock wave in Fig. 5a9–d9 and a14–d14, it was found that the first rebound shock wave was likely stronger than the second one even though the shock speed was slower. It implied that the high pressure that increased inside the minimum bubble volume in the first phase was higher than that of the second phase. The pressure would decrease in the next phase until there is no high pressure inside the bubble volume. That was confirmed by some bubble cloud and suspended jet occurring without any rebounded shock wave as shown in Fig. 5a15–d15 and a16–d16. Such bubble cloud and suspended jet would move upward due to buoyancy force.

Comparison of jet formations between the liquid jets injected in water and air as shown in Figs. 4 and 5, the liquid jets injected in water were much more different from the jet injected in air. The jet in water contained the bubble behaviors while the jet in air did not.

4.2 Liquid jet velocity and jet penetration distance

Figure 6 shows the comparison of average jet velocity and jet penetration distance of high-speed liquid jets injected in both air and water. It was found that the jet velocities of all jets injected in air reached the maximum velocity at the emerging time of 33 μs. Then, the jet velocities rapidly decreased because of aerodynamic drag, while the velocities of all liquid jets injected in water increased and decreased gradually. The average velocities of all jets injected in air were much higher than that in water because aerodynamic drag is much lower than hydrodynamic drag. That affected the jet penetration distances of all jets injected in air being longer than that in water.

Considering the time variation results of jet velocities and penetration distances of water jet in Fig. 6a, the maximum average velocity of 1669.03 m/s was obtained for the water jet injected in air. This value was found to be much higher than that of the water jet injected in water (374.24 m/s). The jet velocity affected to the jet penetration distance as can be seen in the figure that the higher velocity of the water jet injected in air provided the longer the penetration distance compared to that obtained from the water jet injected in water. Similar to the results of other liquid jets in Fig. 6b–d, the liquid jets injected in air provided higher jet velocity and hence longer penetration distance compared to those liquid jets injected in water.

Comparing the results of water jet with other liquid jets injected in air, it was observed that the maximum average velocity of water jet injected in air was the highest value followed by those obtained for gasoline jet (1634.62 m/s, Fig. 6d), kerosene jet (1548.59 m/s, Fig. 6c) and diesel jet (1453.95 m/s, Fig. 6b), respectively. This was because the highest density of water among other liquid jets played a very important role in the speed of liquid jet generation as shown in Table 1. On the other hand, the lower the kinematic viscosity (internal resistance to flow) and the surface tension (the liquid property at surface) of the liquid fuels as

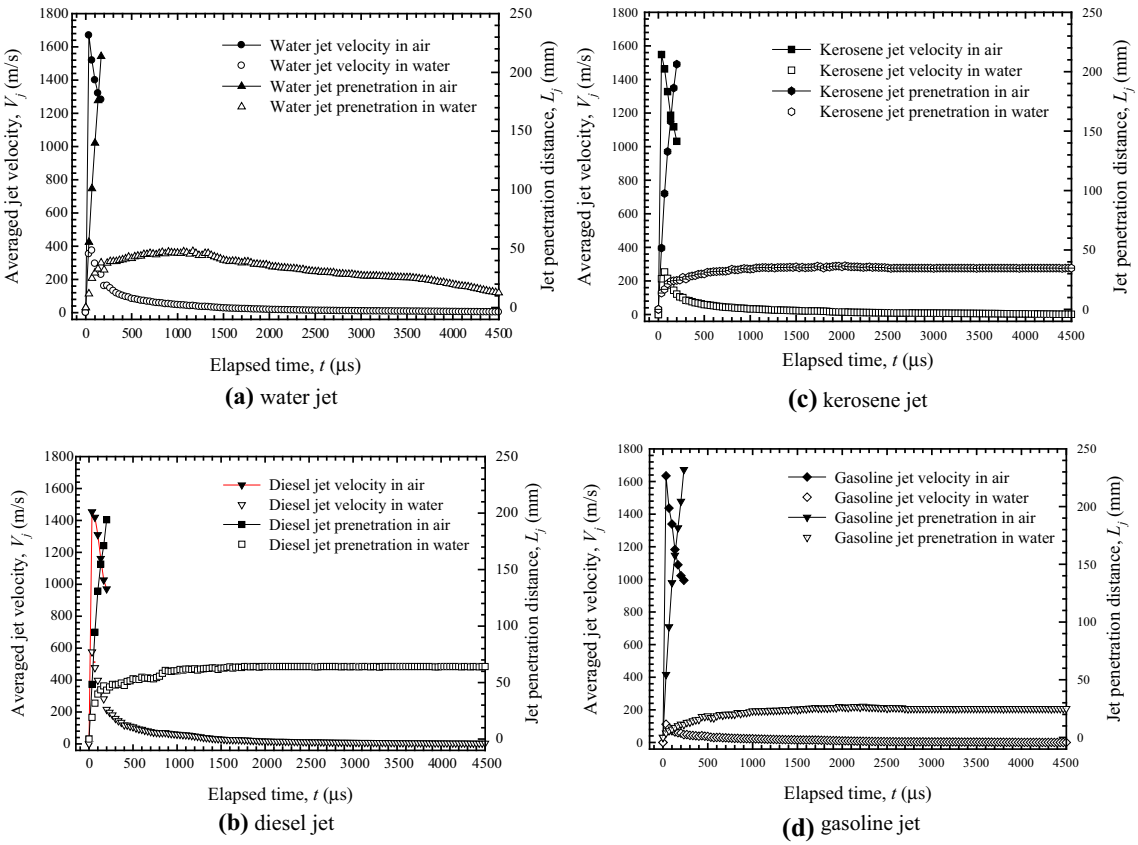

Fig. 6 Comparison of averaged jet velocity and penetration distance of liquid jets injected in air and water

Table 1 Physical properties of liquid

Liquid type	Density at 20 °C (kg/m^3)	Kinematic viscosity at 20 °C (mm^2/s)	Surface tension at 20 °C (kg/s^2)	Heat capacity at 40 °C (J/g °C)	Latent heat (kJ/kg)	The product of surface tension and kinematic viscosity (10^{-6} N m/s)
Water	982.2	1.003	0.0728	4.179	2257.03 (at 100 °C)	0.07302
Diesel	840	4	0.0244	1.97	267.49 (at 170 °C)	0.09760
Kerosene	810	2.5	0.0235	2.02	314.01 (at 117.8 °C)	0.05875
Gasoline	750	0.5	0.02	2.1	318.66 (at 90 °C)	0.01

shown in Table 1, the higher the velocity of the fuel jets. Since the maximum velocity of all jets took place once the jets were injected from the orifice, the kinematic viscosity was found to be a physical property that significantly affected the maximum fuel jet velocity. This was because the liquid fuel jet with lower kinematic viscosity had lower energy loss due to fiction loss between liquid flow and nozzle surface. This was so that the momentum energy from the projectile of the jet with lower kinematic viscosity can be transferred as kinetic energy more than the liquid jet with higher kinematic viscosity.

Considering the slope of each jet velocity trends from 33 to 200 μs, it was found that the trends were significant. The trend of the gasoline jet was steeper than that of kerosene, diesel and water jets. This was because the surface tension of the gasoline jet was lower than that of kerosene, diesel and water jets, respectively. It implied that the lower the surface tension is, the steeper the slope of jet velocity trend is. Hence, it can be concluded that the maximum velocity of high-speed liquid fuel jet in air depends on the kinematic viscosity and its trend depends on the surface tension. The jet velocity affected the jet penetration distance. The greater the velocity, the longer the jet penetration distance of the water jet compared to that of gasoline, kerosene and diesel at each elapsed time as shown in Fig. 6. This occurs because the kinematic viscosity of water was the highest among other jets. At the later elapsed time, the higher the surface tension was, the longer the jet penetration distance was, which was related to the jet velocity.

Unlike the jets injected in air, the jet velocities of all jets injected in water reached the maximum velocity and then gradually decreased mainly because of hydrodynamic drag. The average velocities of all jets injected in water were much lower than that in air because aerodynamic drag is much lower than hydrodynamic drag. That affected the jet penetration distances of all jets injected in water being shorter than that in air. The maximum average velocity of 576.42 m/s (Fig. 6b) for diesel jet injected in water was faster than that of water jet (374.24 m/s, Fig. 6a), kerosene jet (253.80 m/s, Fig. 6c) and gasoline jet (111.84 m/s, Fig. 6d). Moreover, at each elapsed time, the diesel's jet velocity in water was found to be higher than that of water, kerosene and gasoline jets. Considering the results of multiplying kinematic viscosity by surface tension of each liquid as shown in Table 1, it was found that the multiplied result significantly affected the maximum jet velocity at each elapsed time. The higher the multiplied result was, the higher the maximum average jet velocity at each elapsed time was. The jet velocity affected the penetration distance. The greater the velocity, the longer the jet penetration distance of the diesel jet compared to that of water, kerosene and gasoline at each elapsed time. It can be concluded for the liquid jets in water that the higher the multiplied result of kinematic viscosity and surface tension of liquid jet is, the greater the jet velocity and the longer the jet penetration distance are. From Table 1, the derived unit of the product is in N.m/s, which is the unit of power. This might imply that the power of liquid jet plays a significant role for liquid jet injected in water. The stronger the liquid jet power is, the higher jet velocity and jet penetration distance are, while for jets injected in air, this jet power might be dominated and dissipated by atomization and vaporization process. The results of maximum jet velocity including the calculated Mach number and penetration distance of liquid jets injected in water and air can be summarized as shown in Table 2. It is to be informed that the maximum jet velocities obtained from the experiments were at the emerging time of 33 μs only. This limitation is due to the temporal resolution of the imaging device.

Table 2 Maximum jet velocity and penetration distance of liquid jets in air and in water

Jet type	Max. jet velocity (m/s)		Mach no.		Penetration distance (mm)	
	in air	in water	in air	in water	in air	in water
Water	1669.03	374.24	4.91	0.25	213.63	47.89
Diesel	1453.95	576.42	4.28	0.38	194.13	64.23
Kerosene	1548.59	253.80	4.55	0.17	206.31	36.42
Gasoline	1634.62	111.84	4.81	0.07	231.98	26.67

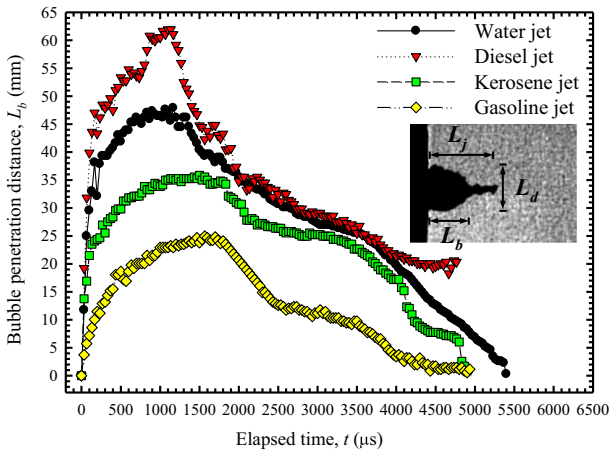

Fig. 7 Bubble penetration distance for liquid jets injected in water

4.3 Bubble penetration distance of liquid jets in water

Unlike the phenomena of liquid jet injected in air, bubble formation was formed during liquid jets injected in water as can be seen in Fig. 5. Figure 7 summarizes a time variation of bubble penetration distance (L_b) of high-speed liquid jets injected in water. At first, the bubble penetration distance (L_b) increased with passage of time as shown in Fig. 7. The maximum bubble penetration distance of diesel jet was longer than that of water, kerosene and gasoline jet, being 61.94 mm, 47.66 mm, 35.84 mm and 24.95 mm at elapsed time of 1100 μs, 1100 μs, 1500 μs and 1567 μs, respectively. From the maximum bubble penetration distance at each elapsed time, the bubble's expansion velocity of diesel was faster than that of water, kerosene and gasoline jets, being estimated to be 56.31 m/s, 43.33 m/s, 23.89 m/s and 15.93 m/s, respectively. After reaching the maximum bubble penetration distance, rapid decrease in bubble penetration distance was clearly observed for diesel jet, while the slower rates of decrease in bubble penetration distance were found for the other jets. The contraction velocity of diesel jet was faster than that of water, kerosene and gasoline jets, being estimated to be 12.24 m/s, 10.04 m/s, 9.04 m/s and 7.20 m/s, respectively. Considering the results of multiplying kinematic viscosity by surface tension of each liquid jet as shown in Table 1, it was found that the multiplied result significantly affected the maximum bubble penetration distance, expansion and contraction velocity in jet penetration direction. The higher the multiplied result was, the higher the maximum bubble penetration distance, expansion and contraction velocities in penetration distance were.

Figure 8 summarizes a time variation of the bubble diameter (L_d) of high-speed liquid jets injected in water. At first, the bubble diameter increased with passage of time. The bubble diameter of the water jet was bigger than that of kerosene, gasoline and diesel jet, being 57.35 mm, 52.19 mm, 48.17 mm and 36.67 mm at 2533 μs, 2300 μs, 2100 μs and 1833 μs, respectively. From the maximum bubble diameter at each elapsed time, the expansion velocity of gasoline was faster than that of kerosene, water and diesel jets, being estimated to be 22.90 m/s, 22.69 m/s, 22.64 m/s and 20.00 m/s, respectively. After reaching the maximum bubble diameter, the decrease in bubble diameter was clearly observed. The bubble contraction of gasoline, kerosene, water and diesel then accelerated at the smallest size of 11.2 mm, 14.39 mm, 18.64 mm and 14.68 mm until 4833 μs, 5100 μs, 5400 μs and 4533 μs, respectively, at which time the minimum bubble diameter corresponds to the minimum bubble penetration distance in Fig. 7. The contraction velocity of the

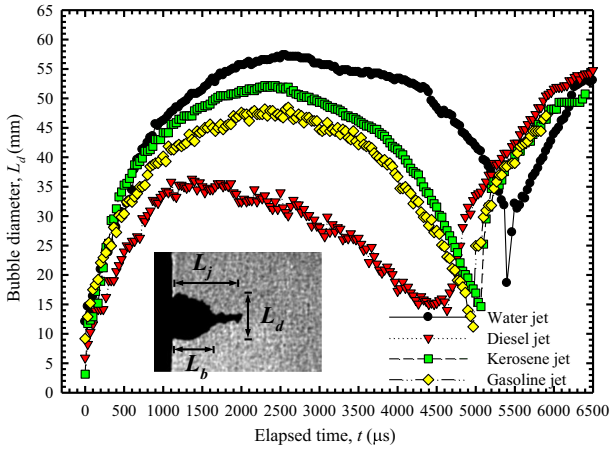

Fig. 8 Bubble diameter

gasoline jet was faster than that of kerosene, water and diesel jets, being estimated to be 13.52 m/s, 13.50 m/s, 13.50 m/s and 8.15 m/s, respectively. The bubble again started to expand at the beginning of the rebound phase. The expansion of the bubble diameter was clearly observed, unlike the bubble penetration as shown in Fig. 7. The bubble diameter, expansion and contraction velocities in bubble diameter increased as the product of surface tension and kinematic viscosity decreased. It can be concluded that the bubble diameter, expansion and contraction velocities in bubble diameter in water depended on the couple effects of kinematic viscosity and surface tension.

5 Conclusions

This study clarifies the comparative effects of liquid properties on characteristics of high-speed liquid jets injected in water and air. A horizontal single-stage powder gun employed the impact-driven method from the same projectile velocity was applied to generate the water, kerosene, diesel and gasoline jets injected in both air and water. Impact-generated high-speed liquid jets were observed by shadowgraph technique. The sequential images were recorded by a high-speed digital video camera. In order to compare the current results with other previous results, the results of jet velocity, jet penetration distance and bubble diameter were presented in dimensional terms. However, further research should be considering the use of non-dimensional terms. The visualization results obtained are summarized as follows:

1. The process of impact-generated high-speed liquid jets injection in air, jet-generated shock waves, change in shock angle and multiple pulse jet was observed. Also, the process of the liquid jets injected in water, jet-induced shock waves, shock propagation, the bubble behavior, bubble collapse-induced rebound shock waves and bubble cloud regeneration was clearly observed.
2. The average velocities of all jets injected in air were much higher than that in water because the aerodynamic drag was much lower than hydrodynamic drag.
3. For liquid jets in water, the maximum average jet velocity, jet penetration distance, bubble penetration distance, expansion and contraction velocities of bubble penetration increased when the product of surface tension by kinematic viscosity increased, representing the couple effect between both physical properties. The maximum average velocity, jet penetration distance, bubble penetration distance, extension and contraction velocities of bubble penetration of diesel jet, representing the highest multiplied result of surface tension by kinematic viscosity, were the highest, being 576.42 m/s, 64.23 mm and 61.93 mm, 56.31 m/s and 12.24 m/s, respectively.
4. Surface tension and kinematic viscosity were found as significant physical properties of jets injected in air and water.
5. If the impact-driven high-speed liquid jet is applied in industrial applications such as underwater work or other related works, transversal direction has to be clearly investigated, not only jet-induced bubble behaviors in longitudinal direction. This is especially the case in medical applications such as the process of removing a cerebral thrombus.

Acknowledgement This research is financially supported by Thailand Research Fund (TRF, Contact No. MRG5180046) and Ubon Ratchathani University. The authors are grateful to W. Sittiwong and K. Pianthong, who assisted in setting up the test facilities.

References

Bourne NK, Field JE (1995) A high-speed photographic study of cavitation damage. J App Phys 78:4423–4427
Bowden FP, Brunton JH (1958) Damage to solids by liquid impact at supersonics speeds. Nature 181:873–875
Bowden FP, Brunton JH (1961) The deformation of solids by liquid impact at supersonic speeds. Proc R Soc Lond 263(1):433–450
Bowden FP, Field JE (1964) The brittle fracture of solids by liquid-impact, by solid impact, and by shock. Proc R Soc London 282:331–352
Charters AC (1987) Development of the high velocity gas dynamics guns. Int J Impact Eng 5:181–203
Crafton J, Carter C, Sullivan J, Elliott G (2006) Pressure measurements on the impingement surface of sonic and sub-sonic jets impinging onto a flat plate at inclined angles. Exp Fluids 40:697–707
Deom A, Gouyon R, Berne C (2005) Rain erosion resistance characterizations, link between on-ground experiments and in-flight specifications. Wear 258:545–551
Ferri A (1964) Review of problems in application of supersonic combustion. J R Aero Soc 68:575–597
Field JE, Lesser MB (1977) On the mechanics of high speed liquid jets. Proc R Soc Lond 357(1):143–162
Glenn LA (1975) The mechanics of the impulsive water cannon. Comput Fluids 3:197–215
Grosch DJ, Riegel JP (1993) Development and optimization of a micro two stage light gas gun. Int J Impact Eng 14:1315–1324
Hawke RS (1989) Hypervelocity projectile acceleration with a railgun using a two-stage gas gun injector. Nucl Instrum Methods Phys Res B40(41):1084–1087
Hirono T, Uenohara H, Komatsu M, Nakagawa A, Satoh M, Ohyama H, Takayama K, Yoshimoto T (2003) Holmium YAG laser-induced liquid jet dissector: a novel prototype device for dissection organs without impairing vessels. Minim Invas Neurosurg 46:121–125
Kennedy CF, Field JE (2000) Damage threshold velocities for liquid impact. J Mater Sci 235:5331–5339
Kobayashi R, Arai T, Yamada H (1988) Structure of a high-speed water jet and the damage process of metals in jet cutting technology. JSME Int J Series B 31:53–57
Lee CS, Park SW (2002) An experimental and numerical study on fuel atomization characteristics of high-pressure diesel injection sprays. Fuel 81(18):2417–2423
Lesser M, Field J (1991) Studies in shock waves, liquid impact, jets and cavitation. In: Takayama K (ed) Proceedings of 1st ISSW, pp 61–72
Matthujak A, Hosseini SHR, Takayama K, Voinovich P (2007) High-speed liquid jet formation by impact acceleration method. Shock Waves 16(6):405–419
Matthujak A, Kasamnimitporn C, Sittiwong W, Pianthong K, Takayama K, Milton BE (2013) Characteristics of impact driven high speed liquid jets in water. Shock Waves 23(2):105–114
Methven TJ, Fairhead B (1959) A correlation between rain erosion of perspex specimens in flight and on a ground rig. Wear 2(6):498–510
Milton BE, Pianthong K (2005a) Pulsed, supersonic fuel jets: a review of their characteristics and potential for fuel injection. Int J Heat Fluid Flow 26(4):656–671
Milton BE, Pianthong K (2005b) Pulsed, supersonic fuel jets: a review of their characteristics and potential for fuel injection. Int J of Heat Fluid Flow 26(4):656–671
Milton BE, Watanabe M, Saito T, Pianthong K (2005) Simulation of supersonic liquid jets using the Autodyne. In: Reddy KP (ed) Proceedings 25th ISSW, India
Nakagawa A, Hirano T, Komatsu M, Sato M, Uenohara H, Ohgawa H, Kusada Y, Shirane R, Takayama K, Yoshimoto T (2002) Holmium: YAG laser-induced liquid jet knife: possible novel method for dissection. Lasers Surg Med 31:129–135
Obara T, Bourne NK, Field JE (1995a) Liquid-jet impact on liquid and solid surfaces. Wear 186–187(2):388–394
Obara T, Bourne NK, Field JE (1995b) Liquid jet impact on liquid and solid surfaces. Wear 186–187:388–394
Ohki T, Nakagawa A, Tominaga T, Takayama K (2004) Experimental application of Pulsed Ho: YAG laser-induced liquid jet as a novel device for rigid neuroendoscope. Laser Surg Med 34:227–234
Ohtani K, Numata D, Takayama K, Kobayashi T, Okatsu K (2009) Experimental study of underwater rock drilling using a pulsed Ho : YAG laser-indued jets. Shock Waves 19:403–412
O'Keefe JD, Wrinkle WW, Scully CN (1967) Supersonic liquid jets. Nature 213:23–25
Pianthong K (2002) Supersonic liquid diesel fuel jets; generation, shock wave; Characteristics, Auto-ignition Feasibilities. Ph.D. Thesis, Univ New South Wales, Sydney, Australia, pp 1–259
Pianthong K, Zakrzewski S, Behnia M, Milton BE (2002) Supersonic liquid jets: their generation and shock wave characteristics. Shock Waves 11(6):457–466
Pianthong K, Milton BE, Behnia M (2003a) Generation and shock wave characteristics of unsteady pulsed supersonic liquid jets. Atom Sprays 13(5&6):475–498
Pianthong K, Zakrzewski S, Milton BE, Behnia M (2003b) Characteristics of impact driven supersonic liquid jets. Exp Thermal Fluid Sci 27(5):589–598
Pianthong K, Takayama K, Milton BE, Behnia M (2005) Multiple pulsed hypersonic liquid diesel fuel jets driven by projectile impact. Shock Waves 14(1&2):73–82
Ryhming IL (1973) Analysis of unsteady incompressible jet nozzle flow. J App Math Phy (ZAMP) 24:149–164
Shi HH, Itoh M (1998) Generation of high-speed liquid jet from a rectangular nozzle. Trans Jpn Soc Aero Space Sci 41(134):195–202

Shi HH, Takayama K (1995) Generation of high-speed liquid jets by high-speed impact of a projectile. JSME Int Ser B J 38(2):181–190
Shi HH, Takayama K (1999) Generation of hypersonic liquid fuel jets accompanying self-combustion. Shock Waves 9(5):327–332
Shi HH, Takayama K, Onodera O (1993) Experimental study of pulsed high-speed liquid jet. JSME Int J 36(4):620–627
Shi HH, Takayama K, Onodera O (1994a) Supersonic diesel fuel injection through a single-hole nozzle in a compact gas gun (part 2). JSME Int J Ser B 37(3):509–516
Shi HH, Field JE, Pickles CSJ (1994b) High speed liquid impact onto wetted solid surfaces. J Fluids Eng 116:345–348
Shi HH, Koshiyama K, Itoh M (1996) Further study of the generation technique of high-speed liquid jets and related shock wave phenomena using a helium gas gun. Jpn J Appl Phys 35(7):4147–4156
Shi HH, Higashiura K, Itoh M (1999) Generation of hypervelocity liquid jets using a powder gun and impact experiment. Trans Jpn Soc Aero Space Sci 42(135):9–18
Shimotani K, Oikawa K, Horada O, Kagawa Y (1996) Characteristics of gasoline in-cylinder direct injection engine. JSAE Rev 17(3):267–272
Soyama H, Yanauchi Y, Sato K, Ikohagi T, Oba R, Oshima R (1996) High-speed observation of ultrahigh-speed submerged water jets. Exp Thermal Fluid Sci 12:411–416
Terao K, Ishii K, Totsuka T, Ishikawa Y (2002) An experimental investigation of hypersonic combustion for Ram jet engine applying detonation waves. In: 11th AIAA/AAAF international conference space planes and hypersonic systems and technologies 2002, Paper No. AIAA-2002–5164
Shi HH (1994) Study of hypersonic liquid jets. Ph.D. thesis, Tohoku University, Sendai, Japan, pp 1–186
Wang Z, Shuai SJ, Wang JX, Tian GH (2006) A computational study of direct injection gasoline HCCI engine with secondary injection. Fuel 85(12–13):1831–1841
Westmark C, Lawless GW (1995) A discussion of rain erosion testing at the United States Air Force rain erosion test facility. Wear 186–187(2):384–387

Publisher's Note Springer Nature remains neutral with regard to jurisdictional claims in published maps and institutional affiliations.